

AD-A069 010

CALIFORNIA UNIV BERKELEY DEPT OF PHYSICS

F/G 8/3

DESCRIPTION OF NONLINEAR INTERNAL WAVE INTERACTIONS USING LANGE--ETC(U)

MAY 79 N POMPHREY, J D MEISS, K M WATSON

N00014-78-C-0050

UNCLASSIFIED

UCB-PTH-79/4

NL

OF  
AD  
A069010



AD A069010

DDC FILE COPY

14 UCB-PTH-79/4

LEVEL

11 May 1979

12 58 p.

6 DESCRIPTION OF NONLINEAR INTERNAL WAVE INTERACTIONS  
USING LANGEVIN METHODS

10 Neil Pomphrey,  
James D./Meiss  
and  
Kenneth M./Watson

DDC  
RECEIVED  
MAY 24 1979  
C

Department of Physics  
and  
Lawrence Berkeley Laboratory  
University of California  
Berkeley, California 94720

15 N00014-78-C-0050

This document has been approved  
for public release and sale; its  
distribution is unlimited.

071 970  
79 05 23 020 mt

# ABSTRACT

A comparison is made between several different methods for calculating energy transport within a wave field. Two Langevin techniques are developed. The first is based on the fluctuation-dissipation theorem and provides relaxation rates  $\nu_F$  and a transport equation. The second method is an application of the Krylov-Bogoliubov-Mitropolsky perturbation theory and provides a Langevin rate constant  $\nu_P$  at lowest order. The two formulations are shown to be closely related to the radiative transfer (Boltzmann) equation whose rate is the difference between  $\nu_F$  and  $\nu_P$ . Specific application of the Langevin methods is to internal waves in the ocean. Computations show that the GM-76 spectrum is approximately an equilibrium spectrum except for frequencies near the inertial frequency and at the lowest vertical modenumbers. The sensitivity of  $\nu_F$  and  $\nu_P$  to spectral form is also discussed. Simple analytic expressions for the rates are derived for the induced diffusion, elastic scattering, and parametric subharmonic instability mechanisms. Only the first of these mechanisms is ever of much numerical significance. Finally, net energy flow in the non-equilibrium portion of the GM-76 spectrum is discussed.

ACCESSION for	
NTIS	White Section <input checked="" type="checkbox"/>
DDC	B. ft Section <input type="checkbox"/>
UNANNOUNCED	<input type="checkbox"/>
CLASSIFICATION	
Ex term 50	
BY	
DISTRIBUTION/AVAILABILITY CODES	
Dist. and/or SPECIAL	
A	

## 1. INTRODUCTION

Nonlinear energy transfer mechanisms within the oceanic internal wave field have been studied by *Olbers* [1976] and *McComas and Bretherton* [1977]. These authors used a radiative transfer equation [*Hasselmann*, 1966, 1967] for their computations. The radiative transfer (or Boltzmann) equation governs the evolution of wave action spectra ensemble averaged over many realizations of the wave field. Derivation of this equation from the fluid equations requires several approximations:

(a) Nonlinearities are assumed "weak," and only lowest order (quadratic for the case of internal waves) nonlinear terms are retained in the equations of motion.

(b) Two-time perturbation methods are used; the "fast time" corresponds to linear wave periods and the "slow time" to nonlinear interaction timescales.

(c) Spatial homogeneity in any horizontal plane is assumed. This allows simplification of second moments of wave amplitudes.

(d) A closure approximation is made by the discard of fourth and higher order cumulants.

In the present study we compare several different techniques for calculating energy transport within the internal wave field. The dynamical

79 05 23 020



equations [Meiss, Pomphrey, and Watson; 1979, henceforth referred to as I] are derived using approximation (a) and describe nonlinear interaction of the linear normal modes of the wave field. Here we use the Garrett-Munk exponential profile for the Väisälä frequency and the WKB approximation to calculate the vertical modefunctions (Olbers [1976] and McComas and Bretherton [1977] have used a constant Väisälä profile). Two Langevin equation techniques are developed in this paper to study the dynamics of the system derived in I (Langevin methods have been used by Holloway and Hendershott [1977] to discuss Rossby waves).

The first Langevin method is based on the fluctuation-dissipation theorem [Lax, 1960, 1966]. This method provides relaxation rates and a transport equation, and depends rather little on dynamics. It assumes linear relaxation to a known equilibrium state and also requires approximations (b), (c) and (d). For the "known equilibrium state," we choose a set of Garrett-Munk related spectra, with the "GM-76" spectrum [Cairns and Williams, 1976] as our reference standard.

To obtain the second form of the Langevin equation we use approximation (b) in the form of the Krylov-Bogoliubov-Mitropolsky perturbation method. [Bogoliubov and Mitropolsky, 1961]. Approximation (d) is not required to calculate the Langevin rate constant with this procedure.

We shall show in Section 3 that the two Langevin formulations are closely related to the radiative transfer equation. For fluctuations near a true equilibrium state the two formulations are in agreement. In this case the transport equation obtained from the Langevin equation is identical in form with that used by Olbers [1976] and by McComas and Bretherton [1977].

The Langevin method leads to a decay rate  $\nu(k)$  for the autocorrelation of the amplitude for a linear internal wave labelled as "k." When calculated using the fluctuation-dissipation theorem, we call this  $\nu_F(k)$ . The value obtained from perturbation theory is written as  $\nu_P(k)$ . The radiative transfer equation used by *Olbers* [1976] and by *McComas and Bretherton* [1977] for the action density  $\langle J_k \rangle$  is of the form

$$\frac{d}{dt} \langle J_k \rangle = 2 \nu_B(k) \langle J_k \rangle ,$$

where

$$\nu_B(k) = \nu_F(k) - \nu_P(k) .$$

It is convenient to think of  $\nu_F$  as representing the rate of energy input to mode k from the "noise field" of the wave system and to think of  $\nu_P$  as describing a rate of energy loss from mode k.

*McComas* [1978] reported numerical experiments in which he introduced small distortions in the GM-76 spectrum and computed the relaxation to "equilibrium." We give an analytic description of this in Section 3 and show that the Langevin autocorrelation decay rate  $\nu_P(k)$  also determines the rate of return to equilibrium.

Numerical calculations of  $\nu_F$  and  $\nu_P$  are presented in Section 5. We shall see that for the GM-76 spectrum, except for frequencies near the inertial frequency and at the lowest vertical mode numbers,  $|\nu_B|$  is from one to three orders of magnitude smaller than  $\nu_F$  (or  $\nu_P$ ). We

thus find precise numerical confirmation of the conclusion of *McComas and Bretherton* [1977] (who calculate only  $v_B$ ) that GM-76 is approximately an equilibrium spectrum.

The sensitivity of  $v_F$  and  $v_P$  to spectral form is also discussed in Section 5 for a class of GM-76 type spectra. Not surprisingly, in the equilibrium region where  $v_B$  is a small difference between two much larger quantities, the values of  $v_B$  are rather sensitive to spectral shape.

*McComas and Bretherton* [1977] describe three limiting mechanisms for energy transfer. They call these induced diffusion, elastic scattering and parametric subharmonic instability. In Section 6 we present simple analytic expressions for  $v_F$  and  $v_P$  for each of these mechanisms. We show from these expressions that GM-76 represents an equilibrium spectrum, except at the lowest frequencies and lowest vertical mode numbers, with respect to both induced diffusion and elastic scattering. (For the case of induced diffusion this was noted by *McComas and Bretherton* [1977] and was implied more generally from their numerical calculations.)

We show that the elastic scattering and parametric subharmonic instability mechanisms are never of much numerical significance for the GM-76 spectrum. For frequencies greater than three times the inertial frequency the analytic expressions obtained from induced diffusion for both  $v_F$  and  $v_P$  agree well with the numerically calculated values for these quantities.

Net energy flow in the non-equilibrium portion of the GM-76 spectrum is discussed in Section 7. Our conclusions are generally consistent with those of *Olbers* [1976] and of *McComas and Bretherton* [1977] that energy

is transferred from the low vertical mode number regime into that of high vertical mode numbers and near inertial frequencies. Since net energy flow is determined by  $\nu_B$ , the details depend relatively sensitively on the assumed spectrum.

The Langevin rate constants discussed here govern relaxation processes in the wave field and also immediately yield values for the more frequently calculated Boltzmann constant  $\nu_B$ . The simple analytic approximations for these rate constants given in this paper should be adequate for applications to internal wave transport processes.



## 2. THE DYNAMICAL MODEL

A general description of internal wave phenomena and theory is given by *Phillips* [1977]. The detailed description of the specific dynamical model used here is given in I. A rectangular coordinate system is chosen with the x-y plane tangent (locally) to the ocean surface. The bottom is assumed horizontal at  $z = -H$ . The Garrett-Munk exponential Väisälä profile is used in this paper:

$$N(z) = N_0 \exp(z/B) \quad . \quad (1)$$

Dimensional quantities are  $N_0 = 5.2 (10)^{-3}$  rad/sec,  $B = 1.2$  km and the surface fluid density  $\rho_0 = \rho(0)$ . The coriolis frequency is assumed vertical with magnitude

$$f = 7.3 (10)^{-5} \text{ rad/sec} = .014 N_0 \quad (2)$$

corresponding to  $30^\circ$  latitude. Vectors,  $\tilde{x} = (x, y)$ , are two-dimensional in the horizontal plane.

The vertical displacement of a Lagrangian fluid element was written in I as

$$\xi_3(\tilde{x}, z, t) = \text{Re} [Y(\tilde{x}, z, t)],$$

$$Y(\tilde{x}, z, t) = i N_0 \sqrt{B} \sum_{\alpha=1}^{\infty} \sum_{\tilde{k}} \frac{a_{\tilde{k}\alpha}(t)}{k} W_{\tilde{k}\alpha}(z) e^{i \tilde{k} \cdot \tilde{x}} \quad (3)$$

Equation (3) is a Fourier expansion in an ocean of rectangular area  $\Sigma_0$



in terms of horizontal wavenumbers  $k$ . The linear vertical modefunctions,  $W_{k\alpha}(z)$ , satisfy the eigenvalue equation

$$\frac{d}{dz} \left[ \rho \frac{d}{dz} W_{k\alpha} \right] + \rho k^2 \left[ \frac{N^2 - \omega_\alpha^2(k)}{\omega_\alpha^2(k) - f^2} \right] W_{k\alpha} = 0,$$

$$\omega_\alpha(k) > 0,$$

$$W_{k\alpha}(0) = W_{k\alpha}(-H) = 0. \quad (4)$$

Here  $\omega_\alpha(k)$  is the angular frequency of a linear internal wave with integer vertical modenumber  $\alpha$ .

The amplitudes  $a_{k\alpha}$  are dimensionless wave slope variables and satisfy [I, eq. 2.23]

$$\dot{a}_k + i\omega_\alpha a_k = \sum_{\ell, m} [\delta_{k+\ell-m} G_{\ell m}^{k\ell} a_\ell^* a_m + \delta_{k-\ell-m} G_{\ell m}^k a_\ell a_m] \quad (5)$$

Here we have used abbreviated labels, writing  $k, \ell, m$  for  $(k, \alpha), (\ell, \beta),$  and  $(m, \gamma)$  respectively. Explicit expressions for the "G" coupling coefficients in (5) were given in I. They contain integrals over the product of three modefunctions  $W$  (see appendix A) as well as factors determined by the geometry of the interacting triad.

Wave action per unit area is expressed in terms of the slope variables as [I, eq. 2.21]

$$J_{k\alpha} = \rho_0 N_0 B^3 \frac{\omega_\alpha N_0}{\omega_\alpha^2 - f^2} \frac{|a_{k\alpha}|^2}{2(kB)^2} \quad (6)$$

The Boussinesq approximation has not been used to derive equations (3), (4) and (5). This approximation entails the neglect of the term  $\frac{dp}{dz} \frac{dW_{k\alpha}}{dz}$  in (4). In Appendix A it is shown to have a negligible effect on the coupling coefficients in (5). We shall therefore make this simplifying approximation for our subsequent discussion.

Following *Garrett and Munk* [1975, 1979] we use the WKB approximation to solve (4). This appears reasonably valid for  $\alpha \geq 2$  (results for  $\alpha=1$  are at best qualitative but will be included for completeness). We also use their dispersion relation

$$\omega_{\alpha}^2(k) = r^2 + \left( \frac{kBN_0}{(\alpha - \frac{1}{2})\pi} \right)^2, \quad (7)$$

valid when  $\omega_{\alpha}(k) \ll N_0$  (and assumed valid in this paper for  $\omega_{\alpha}(k) < N_0/3$ ).

The power spectral density (PSD) of vertical displacement is written as  $\psi(k, \alpha, z)$  and normalized so that

$$\langle \xi_3^2 \rangle = \sum_{\alpha=1}^{\infty} \int d^2k \psi(k, \alpha, z), \quad (8)$$

where " $\langle \rangle$ " represents an ensemble average over realizations of the internal wave field. We shall require only the spectrum  $\psi(k, \alpha)$  extrapolated to the surface for which  $\langle \xi_3^2 \rangle = \langle \xi_0^2 \rangle = (7.3m)^2$ . From equations (1), (3), (6), (7) and the normalization of the eigenfunctions  $W_{k\alpha}$  (Appendix A), we see that

$$\psi(k, \alpha) = \frac{\Sigma_0}{4\pi^2} \frac{\langle |a_{k\alpha}|^2 \rangle}{2k^2}. \quad (9)$$

In this paper we adopt a PSD related to the Garrett-Munk form [Garrett and Munk, 1975, 1979], with

$$\psi(k, \alpha) = \frac{1}{2\pi} N_{pt} \langle (\xi_o B)^2 \rangle \left\{ \frac{(kB)\alpha^{p-1}}{[(kB)^2 + 1.9 (10)^{-3} \alpha^2]^{p/2 + 1} [1 + (\alpha/3)^t]} \right\}, \quad (10)$$

where  $p$  is the "wavenumber slope" and  $t$  is the "modenumber slope." The GM-76 spectrum [Cairns and Williams, 1976] with  $p=2$ ,  $t=2$ , and  $N_{22} = .013$  is chosen as our "standard."

### 3. RELAXATION RATES

In this section we discuss and relate three different methods for calculating relaxation rates in a random wave field. We fix attention on a single, definite internal wave mode, say that labelled  $(k, \alpha)$ . This is the "test wave," and we study its interaction with the ambient wave-field. Averages are denoted " $\langle \rangle$ " and are over an ensemble of states of the ambient field. We suppose that the test wave always has a definite amplitude at some initial time, say  $t=0$ . As  $t \rightarrow \infty$  there will be no difference between this ensemble and an ensemble of states of the entire internal wave field (including the test wave).

#### A. Fluctuation Dissipation Theorem

We cast the equations of motion (5) for the test wave as a Langevin equation by representing the nonlinear terms on the right hand side by a random force  $\tilde{R}(t)$  (for convenience we temporarily drop the mode labels  $(k, \alpha)$ ):

$$\dot{a} + i\omega a = \tilde{R}(t) \quad . \quad (11)$$

From this point of view the test wave is driven by the ambient waves which act as an "equilibrium heat bath." It is convenient to transform variables, defining

$$b(t) = e^{i\omega t} a(t) ; \quad (12)$$

so that (11) becomes

$$\dot{b} = e^{i\omega t} \tilde{R} \equiv R(t) . \quad (13)$$

Following the conventional argument [Lax, 1960, 1966] we suppose that at  $t=0$ ,  $b$  has the definite value  $b(0)$ . The mean of  $b$ , averaged over the ambient ensemble, obeys the equation

$$\frac{d}{dt} \langle b \rangle = \langle R(t) \rangle .$$

It is anticipated that as  $t \rightarrow \infty$ ,  $\langle b \rangle \rightarrow 0$ . This leads to a reasonable postulate for the form of  $R$ :

$$R(t) = -\nu b(t) + F(t) ,$$

$$\langle F \rangle = 0 . \quad (14)$$

Here  $\nu$  is the Langevin relaxation rate (assumed real since any imaginary part may be removed by a transformation of the form (12)).

From assumption (14), equation (13) becomes

$$\dot{b} + \nu b = F(t) \quad (15)$$



from which it follows that

$$\langle b(t) \rangle = b(0) e^{-\nu t} , \quad (16)$$

To develop the fluctuation dissipation theorem we assume

$$\lim_{t \rightarrow \infty} \langle |b(t)|^2 \rangle = \sigma , \quad (17)$$

a constant, equilibrium value. (Since the hamiltonian from which equation (5) was derived has no lower bound in energy, a true equilibrium in the thermodynamic sense does not exist. However, large amplitude fluctuations are sufficiently rare that we can ignore this problem. Note the analogy with the theory of low-lying Stark states of hydrogen.) It is, of course, of interest to determine if the Garrett-Munk PSD (10) corresponds to this equilibrium, and this is one of the tasks for the computations in Sec. 5.

Considerable simplification results by assuming  $\delta$ -correlation of the noise

$$\langle F(t) F^*(t') \rangle \cong 2D \delta(t-t') . \quad (18)$$

Numerical investigations described later indicate that decorrelation is sufficiently rapid that equation (18) is a good approximation for our application. It is easy to show that  $D$  is real.

Integration of (15) using assumptions (17) and (18) and restoring mode labels yields the fluctuation-dissipation result

$$v_F(k, \alpha) = \frac{D(k, \alpha)}{\sigma_{k\alpha}}, \quad (19a)$$

where the subscript "F" indicates that this relaxation rate is derived by the fluctuation-dissipation method.

For future comparison with the radiative transfer equation we generalize (19a) to define a rate coefficient

$$\hat{v}_F(k, \alpha) = \frac{D(k, \alpha)}{\langle |a_{k\alpha}|^2 \rangle}, \quad (19b)$$

where  $\langle |a_{k\alpha}|^2 \rangle$  does not necessarily represent an "equilibrium" value.

To evaluate D we use the linear approximation for the ambient field amplitudes on the right hand side of (5)

$$a_{l\beta}(t) = a_{l\beta}(0) e^{-i\omega_\beta t}.$$

We also use the cumulant discard approximation to reduce fourth moments to second moments. Evaluation is straightforward, giving

$$\begin{aligned} D(k, \alpha) &= \frac{1}{2} \int_{-\infty}^{\infty} \langle F(t) F^*(0) \rangle dt \\ &= \pi \sum_{l, m} \{ |G_m^{kl}|^2 \delta_{k+l-m} \delta(\omega_\alpha + \omega_\beta - \omega_\gamma) \\ &\quad + 2 |G_{lm}^k|^2 \delta_{k-l-m} \delta(\omega_\alpha - \omega_\beta - \omega_\gamma) \} \langle |a_{l\beta}|^2 \rangle \langle |a_{m\gamma}|^2 \rangle. \end{aligned} \quad (20)$$

For a large ocean area  $\Sigma_0$  we may replace wavenumber sums by integrals with the substitution

$$\sum_{\underline{\ell}} \rightarrow \frac{\Sigma_0}{4\pi^2} \int d^2\ell$$

and use equations (20) and (9) to re-write (19b):

$$\begin{aligned} \hat{v}_F(\underline{k}, \alpha) = 2\pi \sum_{\beta, \gamma} \int d^2\ell d^2m \{ & |G_m^{k\ell}|^2 \delta(\underline{k} + \underline{\ell} - \underline{m}) \delta(\omega_\alpha + \omega_\beta - \omega_\gamma) \\ & + 2|G_{\ell m}^k|^2 \delta(\underline{k} - \underline{\ell} - \underline{m}) \delta(\omega_\alpha - \omega_\beta - \omega_\gamma) \} \frac{\ell_m^2}{k^2} \\ & \times \frac{\psi(\underline{\ell}, \beta) \psi(\underline{m}, \gamma)}{\psi(\underline{k}, \alpha)} \end{aligned} \quad (21)$$

It is clear that  $\hat{v}_F$  is a positive quantity.

### B. Perturbation Method

The Krylov-Bogoliubov-Mitropolsky [1961] two-time perturbation method provides an alternative means of obtaining a Langevin equation of the form (15) [see e.g. Case, 1966]. For the lowest order perturbation calculation, the cumulant discard assumption is not required since the test wave is a sure quantity at  $t=0$  under the averages. Using an adiabatic "switch on" in the remote past of the right hand side of (5), we obtain a complex "frequency shift"

$$\begin{aligned}
 v_{\sim}(k, \alpha) = & -i \lim_{\eta \rightarrow 0(+)} \sum_{\ell, m} \left\{ \frac{2G_m^{k\ell} G_{\ell k}^m}{\omega_{\alpha} + \omega_{\beta} - \omega_{\gamma} + i\eta} \delta_{\sim k+\ell-\sim m} \right. \\
 & + \frac{G_{\ell}^{km} G_{\ell}^{mk*}}{\omega_{\alpha} - \omega_{\beta} + \omega_{\gamma} + i\eta} \delta_{\sim k-\ell+\sim m} + \left. \frac{2G_{\ell m}^k G_{\ell m}^{m\ell}}{\omega_{\alpha} - \omega_{\beta} - \omega_{\gamma} + i\eta} \delta_{\sim k-\ell-\sim m} \right\} < |a_{\ell\beta}^{(0)}|^2 > .
 \end{aligned}
 \tag{22}$$

The real part of this is the relaxation rate

$$\begin{aligned}
 v_P(k, \alpha) = & \text{Re}[v_{\sim}(k, \alpha)] \\
 = & -2\pi \sum_{\beta, \gamma} \int d^2 \ell d^2 m \left\{ 2G_m^{k\ell} G_{\ell k}^m \delta_{\sim k+\ell-\sim m} \delta(\omega_{\alpha} + \omega_{\beta} - \omega_{\gamma}) \right. \\
 & + G_{\ell}^{km} G_{\ell}^{mk*} \delta_{\sim k-\ell+\sim m} \delta(\omega_{\alpha} - \omega_{\beta} + \omega_{\gamma}) \\
 & \left. + 2 G_{\ell m}^k G_{\ell m}^{m\ell} \delta_{\sim k-\ell-\sim m} \delta(\omega_{\alpha} - \omega_{\beta} - \omega_{\gamma}) \right\} \ell^2 \psi(\ell, \beta) .
 \end{aligned}
 \tag{23}$$

Here we have used the standard relation

$$\text{Re} \left[ \lim_{\eta \rightarrow 0(+)} \frac{i}{x + i\eta} \right] = \pi \delta(x)$$

and also expression (9) for the PSD. In Appendix (B), equation (23) is re-written in a form which shows that the first and last terms are positive while the second term is negative.

### C. Radiative Transfer Equation

The radiative transfer or Boltzmann equation has been used by *Olbers* [1976] and *McComas and Bretherton* [1977] to describe nonlinear internal wave interactions. In this method, the equations of motion (5) are used to obtain an equation for  $d\langle |a_k|^2 \rangle / dt$  [see, for example, *Davidson*, 1972] in terms of  $\langle a_k a_\ell a_m^* \rangle$ , etc. Equations for the rate of change of these third order moments involve fourth moments. Closure results from discard of fourth order cumulants, leaving second order moments. Use of the homogeneity assumption allows expression of these in terms of the PSD. Finally, first order perturbation theory is used to integrate the equations for  $\langle a_k a_\ell a_m^* \rangle$ . The result of all this is the transport equation

$$\frac{d}{dt} \langle |a_{k\alpha}|^2 \rangle = 2v_B(k, \alpha) \langle |a_{k\alpha}|^2 \rangle \quad (24a)$$

where

$$v_B = \hat{v}_F - v_P \quad (24b)$$

The expression (21) and (23) for  $\hat{v}_F$  and  $v_P$  are to be used here. Symmetry properties of the G-coefficients may be used to rewrite (24) in precisely the form given by *Olbers* [1976] and *McComas and Bretherton* [1977] (Appendix B).

Equation (24) shows the relationship of the Boltzmann transport equation to the two versions of the Langevin description. We shall see in the next section that (24) may also be derived directly from the Langevin equations.



In the application of the fluctuation-dissipation theorem, we were required to assume that the  $\langle |a_{\tilde{k}\alpha}|^2 \rangle$  corresponded to the equilibrium state  $\sigma_{\tilde{k}\alpha}$ . This was not, of course, used to obtain equations (23) and (24), which result from dynamical equations. We see from (24), however, that if  $\langle |a_{\tilde{k}\alpha}|^2 \rangle = \sigma_{\tilde{k}\alpha}$ , then  $v_B(\tilde{k}, \alpha) = 0$  and

$$\hat{v}_F(\tilde{k}, \alpha) = v_F(\tilde{k}, \alpha) = v_P(\tilde{k}, \alpha) \quad . \quad (25)$$

The two forms of the Langevin equation and the transport equation (24) are then consistent. We have seen that the quantity  $\hat{v}_F$  is always positive. Evidently, for an equilibrium spectrum  $v_P$  must also be positive although this is not guaranteed since the full expression (23) for  $v_P$  is not positive definite.

When the ambient field is at (or nearly at) equilibrium, so  $v_P > 0$ , the fluctuation-dissipation "noise"  $D$  tends to excite the mode  $(\tilde{k}, \alpha)$  at a rate  $v_F$  (or  $\hat{v}_F$ ). Energy is lost to the ambient field at the rate  $v_P$ . To illustrate the implications of this, suppose that our test wave has arbitrary initial amplitude, but all other modes are in equilibrium. We can then use (19b) to integrate (24):

$$\langle |a_{\tilde{k}\alpha}(t)|^2 \rangle = \langle |a_{\tilde{k}\alpha}(0)|^2 \rangle e^{-2v_P t} + \frac{D}{v_P} \left( 1 - e^{-2v_P t} \right) \quad . \quad (26)$$

The equilibrium value is evidently

$$\langle |a_{\tilde{k}\alpha}|^2 \rangle = \frac{D(\tilde{k}, \alpha)}{v_P(\tilde{k}, \alpha)} \quad ,$$

as required by the fluctuation-dissipation theorem and (25). Now, from (16), we obtain

$$\langle a_{\vec{k}\alpha}(t) a_{\vec{k}\alpha}^*(0) \rangle = \langle |a_{\vec{k}\alpha}(0)|^2 \rangle e^{-\nu_F t - i\omega_\alpha \times t} \quad (27)$$

So from (26), the time scale for  $\langle |a_{\vec{k}\alpha}|^2 \rangle$  to reach equilibrium is determined by  $\nu_P$ , while the autocorrelation function (27) decay rate is determined by  $\nu_F$ .

The dynamical calculations reported in I, corresponding to numerical integration of equations (5) seem to be reasonably consistent with (26): A test wave of initially small amplitude was found to grow to the GM-76 value in roughly the expected time. It remained at this level as long as the calculation was continued.

In the above discussion we assume that there exists an equilibrium solution to (24). For this to have physical interest the solution should correspond, to some extent, to observed internal wave spectra. In Section 5 we shall present computed values of  $\hat{\nu}_F$  and  $\nu_P$  for a class of GM spectra and conclude as did *McComas and Bretherton* [1977] that GM-76 is nearly an equilibrium spectrum, except for frequencies close to the inertial frequency and for the lowest mode numbers. Within the "equilibrium range" we will see that  $\nu_B$  may be several orders of magnitude smaller than  $\hat{\nu}_F$ , and therefore tends to be quite sensitive to details of the spectrum.

#### 4. FOKKER-PLANCK EQUATION

The assumption that the "noise" term in (15) represents a Markoff process, fluctuating rapidly on the time scale  $\nu_F^{-1}$ , permits one to derive a Fokker-Planck equation for the probability distribution of the amplitude  $b$  [Chandrasekhar, 1943; Wang and Uhlenbeck, 1945]. To obtain this, we first write  $b$  in terms of its real and imaginary parts,

$$b = x + i y \quad .$$

The probability density for  $x$  and  $y$  at time  $t$  is written as  $P(x,y,t)$ .

The Fokker-Planck equation is obtained from (15):

$$\begin{aligned} \frac{\partial P}{\partial t} = & \frac{\partial}{\partial x} [\nu_F x P] + \frac{\partial}{\partial y} [\nu_F y P] \\ & + \left( \frac{\partial^2}{\partial x^2} + \frac{\partial^2}{\partial y^2} \right) \left[ \frac{DP}{2} \right] , \end{aligned} \quad (28)$$

Here  $D$  is the quantity defined by (20). An equation of evolution for the wave amplitude intensity

$$\langle |a|^2 \rangle = \int (x^2 + y^2) P \, dx dy$$

may be obtained immediately from (28):

$$\frac{d}{dt} \langle |a_{k\alpha}|^2 \rangle = 2\nu_F(k,\alpha) [\sigma_{k\alpha} - \langle |a_{k\alpha}|^2 \rangle] \quad . \quad (29)$$

This is precisely equivalent to (24) if there exists an equilibrium spectrum  $\sigma$ , since then  $v_F = v_P$ . In Appendix B (29) is rewritten to include the effects of inhomogeneous media.

We have now introduced three different rate constants,  $v_P$ ,  $v_F$ , and  $v_B$ . It is to be observed from equations (24), (26), (27) and (29) that  $v_B$  describes the net rate of transfer of action (or energy), whereas  $v_P$  (or  $v_F$ ) represents a relaxation rate.

## 5. COMPUTATIONS AND RESULTS

In this section we evaluate (21) and (23) for  $\hat{v}_F$  and  $v_P$  for given test wave parameters (wavenumber, frequency and modenumber). The coefficients  $G$  depend on integrals over WKB modefunctions  $W_{k\alpha}$ . In Appendix A we show that to a good approximation the modenumber dependence of these integrals can be replaced by a delta function condition (corresponding to approximate vertical wavenumber conservation). This greatly simplifies the evaluation of the decay rates since use of the delta functions reduce their calculation to a single sum over modenumber (selects individual frequency resonance curves) and a single integral along each curve.

The wavenumber conservation relations restrict the allowed region of triad interaction to an open rectangle in  $m$ - $l$  space such as shown in Figure 1. The frequency resonance conditions further restrict allowed interactions to simple curves within the rectangle. If we neglect the Coriolis frequency  $f$  in the dispersion relation (7), the resonance curves are straight lines whose slope and intercept depend on modenumber ratios. With  $f \neq 0$  the curves are bent to an extent which depends on the proximity to the  $m$  and  $l$  axes and on the value of  $k$ . Two examples of resonance curves are illustrated in Figure 1.

The parameter range for the calculations is determined by the region of validity of the WKB model. We allow frequencies in the range  $f < \omega < N_0/3$  where the upper limit may be varied to test for sensitivity of results. If any member of a wave triad has a frequency greater than the cut-off value, that triad does not contribute to  $v$ . Similarly, we employ a long wavelength cut-off at 100 km so that the "plane ocean" assumption remains



valid. For satisfactory convergence ( $\sim 5\%$ ) of the values for  $\nu$  it was sufficient to retain only modenumbers in a band of halfwidth 25 centered about the test wave modenumber. That is, triads lying on resonance curves for which  $|\alpha-\beta|, |\alpha-\gamma| \leq 25$  were included in the calculations.

Changing the value of the frequency cut-off by 25% typically produced less than a 5% change in  $\nu$  for frequencies  $\omega_\alpha < 15f$ . For higher frequencies, important local frequency and wavenumber interactions (induced diffusion, Section 6) are blocked by the cut-off, and the rates are diminished. Quantitative results are found up to  $\approx 17f$  or even higher for large modenumbers. Changing the low-wavenumber cut-off can also have a significant effect ( $\sim$  factor of 2), especially for low modenumbers. This is again due to the induced diffusion mechanism where one triad member has a small wavenumber. The analysis in Section 6 provides a semi-quantitative estimate for the importance of this cut-off.

Figure 2 presents a plot of the decay rate  $\nu_p$  against test wave frequency for the GM-76 PSD (10). Each solid curve is labelled by the test wave modenumber  $\alpha$ . The heavy dashed line represents equality between decay rate and linear frequency, and therefore distinguishes regions of weak and strong nonlinearity (below and above the line, respectively). Since the theory assumes a weakly nonlinear wavefield, little quantitative reliability can be placed on results above the dashed line. The high frequency "kink" in the curves is a result of the frequency cut-off at  $21f$ .

The results show some common trends and features. For given test wave frequency, waves with large modenumber (wavenumber) decay most rapidly: For given modenumber, the higher frequency (wavenumber) waves

decay fastest, and there is a low frequency threshold ( $\omega_\alpha \approx 3f$ ) below which the decay rate decreases very rapidly with decreasing frequency. These features are also exhibited in Figure 3 which presents the same results as Figure 2 except  $v_p$  is plotted as a function of wavenumber. At high frequencies, a common (modenumber independent)  $k$ -dependence for the decay rate is apparent.

It was noted in Section 3 that the expression (23) for  $v_p$  is not positive definite: Interactions for which  $\omega_\alpha = \pm(\omega_\beta - \omega_\gamma)$  ("difference reactions") have the possibility of giving rise to initial growth of the test wave amplitude. It is clear that if  $\omega_\alpha < 2f$ , difference reactions are the only type of interactions possible; therefore  $v_p$  is most likely to be negative at these low frequencies. Indeed our results show growth (negative  $v_p$ ) for small frequencies, especially at high modenumbers. This is indicated in Figure 4 which is a contour plot of the rate calculations. Here the shaded region corresponds to growth, the remainder decay.

The calculation of the fluctuation-dissipation decay rate  $\hat{v}_F$  is essentially the same as for  $v_p$ , and the same cut-off parameters were used. Numerical estimates of the correlation time  $t_c$  for the "noise" term  $F$  in equation (15) show that  $t_c \sim \omega_\alpha^{-1}$  so that the delta correlation assumption (18) is valid in the same region as the weak nonlinearity assumption,  $\hat{v}_F < \omega_\alpha$ .

In Section 3 we saw that if  $\psi$  is an equilibrium PSD for the mode  $(k, \alpha)$  then  $v_F(k, \alpha) = v_p(k, \alpha)$ . Similarly, if the wave field is nearly in equilibrium, then  $v_B = \hat{v}_F - v_p$  is "small." An appropriate measure of

relative equilibrium is not  $v_B$  itself but rather the ratio

$$R(k, \alpha) \equiv \frac{|v_B|}{v_F} \quad (30)$$

which compares the timescale for evolution of the spectrum to that for relaxation of a single mode.

The ratio  $R$  is plotted against  $\omega_\alpha$  for selected  $\alpha$  in Figure 5 using the GM-76 PSD. Apart from a sharp increase in  $R$  at low frequencies and at high modenumbers (associated with  $v_p < 0$ ), the small size of  $R$  over such a wide range of  $\omega_\alpha$  and  $\alpha$  is supportive evidence that GM-76 is a "good" representation of an equilibrium spectrum. Below we will compare GM-76 with other spectral forms to test the sensitivity of this result.

*Olbers* [1976] and *McComas and Bretherton* [1977] have calculated energy transfer rates for various GM models. They have also determined the direction of the energy flow by mapping regions of positive and negative  $v_B$ . We investigate the effect of the variation of two parameters in the PSD. Using GM-76 as the basic form for  $\psi$  [see equation (10)], we change the wavenumber slope "p" and the modenumber slope "t."

#### A. Wavenumber Slope Change

With the modenumber slope given by the reference GM-76 value ( $t=2$ ) we compute the ratio  $R$  for six values of the wavenumber slope. The results are presented as contours in  $(\omega_\alpha, \alpha)$  space in Figure 6. Regions for which  $R > 1$  are designated "non-equilibrium" and shaded to indicate the sign of  $v_B$ . Energy flows from regions of negative (decay)

to positive (growth)  $v_B$ . When  $R < .1$ , contours of  $R$  are plotted and the sign of  $v_B$  is ignored. The area of this region and of the region  $R < .01$  indicates how much of the spectrum is equilibrium.

The GM-76 PSD ( $p=2$ ) is in equilibrium except for low modenumbers ( $\alpha < 7$ ) where the action decays and for low frequencies and high modenumbers ( $\omega < 2.5f$ ,  $\alpha > 7$ ) where the action grows. Decreasing  $p$  extends the  $v_B > 0$  region to lower modenumbers and higher frequencies; increasing  $p$  has the opposite effect. Overall, GM-76 is closest to equilibrium in the high wavenumber region, although the results for smaller slopes are not very different.

#### B. Modenumber Slope Change

Here the procedure is the same as above except that the wavenumber slope is fixed at the GM-76 value ( $p=2$ ), and the modenumber parameter  $t$  is varied. Figure 7 shows the results in the same format as Figure 6. Unlike the previous case, as  $t$  decreases the growth region is confined to higher modenumbers while the decay region expands. The GM-76 spectrum is again more closely in equilibrium for high wavenumbers than the other spectra, although for  $2 < t < 3$  there is little change in the equilibrium region.

Generally, the equilibrium region  $\alpha > 5$  and  $\omega_\alpha > 3f$ , is insensitive to the slope parameters  $p$  and  $t$ . However, these parameters strongly affect the division between regions of growth and decay of the action. For GM-76 our computations are in agreement with McComas and Bretherton indicating that action flows from  $\alpha \lesssim 5$  into  $\alpha \gtrsim 10$  and  $\omega_\alpha \lesssim 3f$ .



## 6. SPECIAL TRANSFER MECHANISMS

McComas and Bretherton [1977] have emphasized that certain classes of triads have significant roles in determining transfer rates. In this section we shall discuss quantitatively the importance of these mechanisms for both the Langevin and Boltzmann rate constants.

We begin with a discussion of the mechanisms called induced diffusion and elastic scattering by McComas and Bretherton. We discuss these together as limiting case I (LCI). As previously, we let  $(k, \alpha)$  be the test wave; then LCI corresponds to the triad conditions

$$\omega_Y(m) \approx \omega_\alpha(k) \gg \omega_\beta(l),$$

$$m \approx k \gg l. \quad (31)$$

In this limiting case the G coefficients have simple forms, and we may re-write (21), (23), and (24b) as

$$\begin{aligned} v_x(k, \alpha) = & \frac{\pi}{2} B N_0 \frac{[\omega_\alpha^2(k) - f^2]^2}{k^2} \sum_{\beta, \gamma} \frac{\omega_Y^2(k) - f^2}{\omega_Y(k)} \frac{A_x}{\psi(k, \alpha)} \\ & \times \int_{l < k} d^2 l \psi(l, \beta) \frac{\omega_\beta^2(l)}{l^2} v_{k\alpha, l\beta, k\gamma}^2 \sum_{\pm} \delta[\omega_\alpha(k) - \omega_Y(k) \pm \omega_\beta(l)]. \end{aligned} \quad (32)$$

The index "x" is used to represent "P", "F", or "B" where

$$A_P \equiv \frac{N_o \omega_\alpha(k)}{\omega_\alpha^2(k) - f^2} \psi(k, \alpha),$$

$$A_F \equiv \frac{N_o \omega_\gamma(k)}{\omega_\gamma^2(k) - f^2} \psi(k, \gamma),$$

$$A_B \equiv A_F - A_P \quad . \quad (33)$$

From (6) and (9) it is seen that  $A_P$  is proportional to wave action. The quantity  $v_{k\ell k}$  is the overlap integral of vertical modefunctions evaluated in Appendix A.

Equations (32) and (33) show that for LCI triads, the equilibrium condition  $v_B = 0$  corresponds to

$$A_F = A_P \quad (34)$$

or that  $A$  be independent of modenumber (equipartition of action).

(For the case of induced diffusion this was noted by *McComas and Bretherton* [1977]). The results (32) and (34) do not require either the WKB or Boussinesq approximations. The WKB dispersion relation (7) yields for (34)

$$\psi(k, \alpha) \sim \alpha^{-1}$$

except near the inertial frequency which is precisely the form of GM-76 (10) in this domain and for  $\alpha \gg 3$ . The numerical calculations

in the previous section show equilibrium in this same region. We shall show in the following that this is because LCI triads dominate the wave interactions.

The integral  $v_{k\ell k}$  appearing in (32) is evaluated in the WKB approximation in Appendix A. From this we see that

$$v_{k\ell k}^2 \propto [\delta_{\alpha-\beta-\gamma} + \delta_{\alpha+\beta-\gamma} + \delta_{\alpha-\beta+\gamma}] \quad (35)$$

(For our actual calculations we use the more accurate form given in the Appendix.) The terms  $\beta = \pm(\alpha-\gamma)$  when  $\gamma \approx \alpha \gg \beta$  correspond to induced diffusion (ID). The term  $\beta = \alpha+\gamma$  corresponds to elastic scattering (ES).

Analytic evaluation of (32) for these two cases gives the expressions

Induced diffusion:

$$\frac{v_P}{N_0} = 6.4 \times 10^{-4} \frac{(\alpha - \frac{1}{4})^3 (\beta - \frac{1}{4})^2 \omega_\alpha}{\left(1 - \frac{\pi \omega_\alpha}{2N_0}\right)^6 \beta^2 (\beta^2 + 9) N_0},$$

$$\beta = \frac{1}{4} + \frac{(\alpha - \frac{1}{4}) f \omega_\alpha}{(\omega_\alpha^2 - f^2)}; \quad (36)$$

Elastic scattering:

$$\frac{v_P}{N_0} = 1.0 \times 10^{-5} \frac{(kB)^3 N_0^2 \omega_\alpha}{\left(1 - \frac{\pi \omega_\alpha}{2N_0}\right)^3}$$

$$\times \sum_{+,-} \frac{(\beta - \frac{1}{4})^2}{\beta^2 (\beta^2 + 9) (\omega_\gamma^2 - f^2)^{3/2} \left(1 - \frac{\pi \omega_\gamma}{2N_0}\right)^3}, \quad (37)$$

$$\beta = \frac{1}{4} + (\alpha - \frac{1}{4}) \left[ 1 + \sqrt{\frac{\omega_{\alpha}^2 - f^2}{\omega_{\gamma}^2 - f^2}} \right] . \quad (37)$$

The sum "+,-" above represents the sum over the two cases

$$\omega_{\gamma} = \omega_{\alpha}(k) \pm f . \quad (38)$$

For the analytic evaluation of (36) and (37) the upper limit of the integral over  $\ell$  in (32) has been taken to be infinity since this has little effect on the result. The numerical calculations reported in Section 5 use a lower limit  $\ell_{\min} = 2\pi/(100\text{km})$ . This results in the multiplication of expressions (36) and (37) by a factor  $[1 - \frac{2}{\pi} \tan^{-1}(\ell_{\min} N_0/\beta\pi f)]$ .

In Figure 8 we compare the ID expression (36) (dashed curve) with the calculated numerical results (solid curve) for  $v_p$  (for this comparison the  $\ell$ -integral cut-off was included). It is evident that except for  $f < \omega \leq 3f$ , the ID mechanism provides a very good approximation for  $v_p$ , and that  $v_p$  may be easily calculated from the analytic expression (36).

In Figure 9 we compare the ES (36) and ID (39) expressions for  $v_p$ . It is seen that ES is much less important than ID.

The parametric subharmonic instability (PSI) mechanism of *McComas and Bretherton* [1977] corresponds to a large scale double frequency wave



interacting with two smaller scale waves with nearly equal frequencies.

In our notation, this corresponds to

$$l \ll k, m \quad ,$$

$$\beta \ll \alpha, \gamma \quad ,$$

$$\frac{\omega_\beta}{2} \approx \omega_\alpha \approx \omega_\gamma \quad . \quad (39)$$

Since the ID mechanism successfully accounts for the interactions with

$\omega_\alpha \gtrsim 3f$ , we expect that, at most, PSI could be important in the region

$\omega_\alpha \lesssim 2f$ . For this case we find

$$v_P \approx -v_F \quad (40)$$

and an analytic evaluation is again possible. In contrast to the ID and ES derivations a finite upper limit must be imposed on the  $l$ -wavenumber integration for convergence of the approximate expressions. With the choice  $l_{\max} = k/5$  the PSI limit for  $v_P$  was one to two orders of magnitude less than the full computation for the range  $f < \omega_\alpha < 2f$ . Simulation of the PSI conditions (39) in the full numerical code has shown that, although the frequency and modenumber limiting conditions were both well satisfied by the important triads, the wavenumber condition was not. We conclude that for  $f < \omega_\alpha < 2f$  the important triads have comparable wavenumbers.

Choosing  $\ell_{\max} = k$ , a rather crude approximation for  $v_p$  in the range  $f \leq \omega_\alpha \leq 2f$  can be derived which gives the correct order of magnitude:

$$\frac{v_P}{N_0} \approx - \frac{\hat{v}_F}{N_0} \approx - 3.5 (10)^{-7} \left( 4 - \frac{f^2}{\omega_\alpha^2} \right)^{5/2} [Q - \tan^{-1} Q]$$

$$Q = \frac{kBN_0}{\pi(4\omega_\alpha^2 - f^2)} \quad . \quad (41)$$

Values calculated from (41) are shown in Figure 9.

The conclusions of this section are that for  $\omega_\alpha > 3f$  and  $\alpha \geq 5$ , the ID mechanism, expressed by (36) provides a good description of relaxation within the internal wave field. The ES and PSI mechanisms are never of much importance.

Equation (32), its analytic solution, and the good agreement with the full numerical calculation provide the explanation for the conclusion that the GM-76 spectrum is in equilibrium in the domain  $\omega_\alpha > 3f$  and  $\alpha > 5$ . Outside this domain the spectrum does not seem to be in equilibrium.

## 7. ENERGY FLOW

Three-wave interactions are only one of the many processes which contribute to the overall energy balance in the ocean. To understand the measured internal wave energy spectrum requires a quantitative measure of flow rates between the various sources and sinks. Here we obtain an estimate of the energy flow rate through the non-equilibrium region of GM-76 which also indicates the energy requirements to maintain the spectrum.

The mean energy per unit area  $E(k, \alpha)$  for the test wave is [I, eq. 2.19]

$$E(k, \alpha) = \omega_{\alpha}(k) \langle J_{k\alpha} \rangle \quad (42)$$

The flow rate is obtained by taking the time derivative of (42) using equations (24), (6) and (9):

$$\frac{dE(k, \alpha)}{dt} = \frac{4\pi^2}{\Sigma_0} \frac{2\omega_{\alpha}^2}{\omega_{\alpha}^2 - f^2} v_B \psi(k, \alpha) \rho_0 N_0^2 B \quad (43)$$

Since the radiative transfer equation conserves total energy, the net energy flow from the region  $v_B < 0$  is equal to the flow into  $v_B > 0$ . We compute the flow from the negative region by integrating (43) over this domain of  $k, \alpha$  space:

$$\frac{dE^{(-)}}{dt} = \sum_{\alpha} \frac{dE_{\alpha}^{(-)}}{dt} = \sum_{\alpha} \sum_{\substack{k \\ v_B < 0}} \frac{dE(k, \alpha)}{dt} \quad (44)$$

The calculated partial rates  $dE_{\alpha}^{(-)}/dt$  are given in table 1 for modenumbers between  $\alpha=1$  and  $\alpha=6$ . For the first 5 modenumbers they are comparable, while for  $\alpha=6$  the rate has decreased by nearly a factor of 2, and the contributions from  $\alpha>6$  (not shown) are much smaller. Except for  $\alpha=1$ , the main contribution to the k sum in (44) peaks near  $\omega_{\alpha} \approx 2.2f$ , independent of  $\alpha$ . Although the peak is not sharp it does suggest that the flow through the spectrum to smaller frequencies is weak: The major flow is from low to high modenumbers. The net energy flow rate from the region of negative  $v_B$  sums to  $dE^{(-)}/dt \approx 6.4 (10)^{-4} \text{ W/m}^2$  for  $\alpha \leq 6$ , and we believe that this represents only a slight underestimate of the total rate.

*Olbers* [1976] has evaluated the transfer rate to high modenumbers for the GM-75 spectrum and found it to be  $3 (10)^{-3} \text{ Wm}^{-2}$ , significantly larger than our GM-76 rate. *McComas and Bretherton* [1977], however, have noted a sensitivity of results to spectral shape as is reflected in our Figures 6 and 7. Thus the validity of computed transfer rates certainly depends on the precision to which the spectrum is known.



ACKNOWLEDGMENTS

This research was partially supported by the Office of Naval Research under contract N00014-78-C-0050. The authors wish to express appreciation to Professor W. H. Munk and Mr. P. Yau for helpful discussions.

REFERENCES

- Abramowitz, M., and I. A. Stegun, *Handbook of Mathematical Functions*, National Bureau of Standards, 1964.
- Bogoliubov, N. N., and Y. A. Mitropolsky, *Asymptotic Methods in the Theory of Nonlinear Oscillations*, Gordon and Breach Science Publ., New York, 1961.
- Cairns, J. L. and G. O. Williams, Internal waves from a midwater float, 2, *J. Geophys. Res.*, 81, 1943-1950, 1976.
- Case, K. M., A general perturbation method for quantum mechanical problems, *Prog. of Theor. Phys.*, Supplement Nos. 37 and 38, 1966.
- Chandrasekhar, S., Stochastic problems in physics and astronomy, *Rev. Mod. Phys.*, 15, 1-89, 1943.
- Davidson, R. C., *Methods in Nonlinear Plasma Theory*, Academic Press, N.Y., 1972, pp. 133-173.
- Garrett, C. J. R., and W. H. Munk, Space-time scales of internal waves: A progress report, *J. Geophys. Res.*, 80, 291-297, 1975.
- Garrett, C. J. R., and W. H. Munk, Internal waves in the ocean, in *Annual Rev. of Fluid Mech.*, edited by M. Van Dyke, J. V. Wehausen, and J. L. Lumley, Annual Reviews, Inc., Palo Alto, CA, 1979.
- Garrett, C. J. R., and W. H. Munk, Space-time scales of internal waves, *Geophys. Fluid Dyn.*, 2, 225-264, 1972.
- Hasselmann, K., Feynman diagrams and interaction rules of wave-wave scattering processes, *Rev. Geophys. Space Phys.*, 4, 1-32, 1966.
- Hasselmann, K., Nonlinear interactions treated by the methods of theoretical physics, *Proc. Roy. Soc., Ser. A* 299, 77-100, 1967.

- Holloway, G. and M. Hendershott, Stochastic closure for nonlinear Rossby waves, *J. Fluid Mech.*, 82, 747-765, 1977.
- Lax, M., Fluctuations from the nonequilibrium steady state, *Rev. Mod. Phys.*, 32, 25-64, 1960.
- Lax, M., Classical Noise IV: Langevin Methods, *Rev., Mod. Phys.*, 38, 541-566, 1966.
- McComas, C. H., Equilibrium mechanisms within the oceanic internal wave field, *J. Phys. Oceanography*, 7, 836-845, 1978.
- McComas, C. H., and F. P. Bretherton, Resonant interaction of oceanic internal waves, *J. Geophys. Res.*, 82, 1397-1412, 1977.
- Meiss, J. D., N. Pomphrey, and K. M. Watson, Numerical analysis of weakly nonlinear wave turbulence, *Proc. Natl. Acad. Sci. USA*, 1979, (referred to as I in the text).
- Olbers, D. J., Non-linear energy transfer and the energy balance of the internal wave field in the deep ocean, *J. Fluid Mech.*, 74, 375-399, 1966.
- Phillips, O. M., *The Dynamics of the Upper Ocean*, Cambridge University Press, New York, 1977.
- Wang, M. C., and G. E. Uhlenbeck, On the theory of the Brownian motion, *Rev. Mod. Phys.*, 17, 323-342, 1945.

# APPENDIX A

## OVERLAP INTEGRALS FOR EXPONENTIAL PROFILE

The explicit form of the coupling coefficients  $G$  in the equations of motion (5) is given in the appendix of I. The only Väisälä profile dependent terms in these coefficients are the "overlap integrals":

$$\begin{aligned} v_{k\ell m} &= \frac{1}{\rho_0} \int_{-H}^0 \rho W'_{k\alpha} W'_{\ell\beta} W'_{m\gamma} dz, \\ \mu_{\ell m}^k &= \frac{1}{\rho_0} \int_{-H}^0 \rho W'_{k\alpha} W_{\ell\beta} W_{m\gamma} dz, \end{aligned} \quad (A1)$$

where the modefunctions  $W(z)$  are solutions of (4) with the normalization

$$\frac{1}{\rho_0} \int_{-H}^0 (N^2 - f^2) \rho W_{k\alpha} W_{\ell\beta} dz = \delta_{\alpha\beta}. \quad (A2)$$

The Boussinesq approximation entails setting  $\rho = \rho_0 = \rho(z=0)$  in these integrals as well as in (4). Since typically  $\rho$  varies by only  $\sim 0.3\%$  over the depth of the ocean, this approximation has little effect on the values of the overlap integrals (A1).

In this approximation the eigenvalue problem (4) becomes

$$\begin{aligned} W''_{k\alpha} + Q_{k\alpha}^2(z) W_{k\alpha} &= 0, \\ Q_{k\alpha}^2 &\equiv k^2 \left( \frac{N^2(z) - \omega_\alpha^2}{\omega_\alpha^2 - f^2} \right). \end{aligned} \quad (A3)$$



If we restrict ourselves to the region  $\omega \ll N_0$  the  $\mu_{\ell m}^k$  integral can be neglected. Qualitatively this can be seen by considering the constant profile model

$$N = N_0 \quad B < z < 0 \quad (A4)$$

for which

$$v_{k\ell m} = \frac{1}{N_0^3 \sqrt{2B}} Q_\alpha Q_\beta Q_\gamma \{ \delta_{\alpha-\beta-\gamma} + \delta_{\beta-\gamma-\alpha} + \delta_{\gamma-\alpha-\beta} \} ,$$

$$\mu_{\ell m}^k = \frac{1}{N_0^3 \sqrt{2B}} Q_\alpha \{ -\delta_{\alpha-\beta-\gamma} + \delta_{\beta-\gamma-\alpha} + \delta_{\gamma-\alpha-\beta} \} ,$$

$$Q_\alpha = \frac{\alpha\pi}{B} . \quad (A5)$$

From the form of the coupling coefficients [I, equation (A.2)], it is seen that the ratio of the  $\mu$  to the  $v$  containing terms is given by

$$(k/Q)^2 \sim (\omega/N_0)^2 \ll 1.$$

This result is confirmed quantitatively by numerical evaluation of the overlap integrals for the exponential profile.

To compute  $v_{k\ell m}$ , it is sufficient to use the WKB solutions of (A3) correct to first order in  $\eta = \omega/N_0$ :

$$W_{k\alpha}(z) = \frac{\sqrt{2B}}{N_0} d_{k\alpha} \frac{[1 - \frac{\pi}{2} \eta_\alpha(k)]}{\Delta_\alpha} e^{-z/2B} \sin[\phi(z) + \pi/4] ,$$

where

$$d_{k\alpha} \equiv \left[ \frac{B Q_{k\alpha}^3(0)}{\Delta_\alpha + \frac{1}{2}} \right]^{1/2} , \quad \Delta_\alpha \equiv \pi(\alpha - \frac{1}{4}) ,$$

$$Q_{k\alpha}(z) = \frac{1}{B} \left[ \frac{\Delta_\alpha}{1 - \frac{\pi}{2} \eta_\alpha} \right] \frac{N}{N_0} ,$$

$$\phi(z) = \Delta_\alpha \left[ \frac{\frac{N}{N_0} - \frac{\pi}{2} \eta_\alpha}{1 - \frac{\pi}{2} \eta_\alpha} \right] . \quad (A6)$$

The WKB overlap integral is formed by differentiating  $W_{k\alpha}$  while keeping  $e^{-z/2B}$  fixed, and substituting into (A1). The result is

$$v_{klm} = \frac{1}{N_0^3 \sqrt{2B}} d_{k\alpha} d_{l\beta} d_{m\gamma} \{ I_{lm}^k + I_{mk}^l + I_{kl}^m \} \quad (A7)$$

where

$$I_{lm}^k \equiv (-1)^{\alpha-\beta-\gamma} \sqrt{\frac{\pi}{2q}} [C_2(q) \sin q - S_2(q) \cos q] . \quad (A8)$$

Here  $S_2$  and  $C_2$  are Fresnel Integrals [Abramowitz and Stegun, 1964], and  $q$  is the dimensionless vertical wavenumber mismatch at the surface

$$q = B |Q_{k\alpha}(0) - Q_{l\beta}(0) - Q_{m\gamma}(0)| . \quad (A9)$$

To first order in  $\eta$  this can be written as

$$q = \pi |\alpha - \beta - \gamma + \frac{1}{4} + \frac{1}{2} (\eta_\alpha \Delta_\alpha - \eta_\beta \Delta_\beta - \eta_\gamma \Delta_\gamma)| \quad . \quad (A10)$$

The function  $I_{\ell m}^k$  is peaked about zero vertical wavenumber mismatch. This gives an approximate vertical wavenumber conservation law analogous to that in (A5) for the constant N model. Comparing (A7) with (A5) further shows that  $d_{k\alpha}$  plays the role of effective vertical wavenumber.

A simple functional fit to  $I_{\ell m}^k$  is given by

$$I_{\ell m}^k(q) = \frac{2}{3} e^{-aq^2} \cos(bq)(-1)^{\alpha-\beta-\gamma} \quad , \quad (A11)$$

where  $a = .0453$  and  $b = .3743$ . It involves an error of less than 4% for  $0 \leq q < 4$ .

To facilitate the evaluation of the Langevin decay rates we approximate the function  $I_{\ell m}^k$  with a delta function, thereby enabling one of the modenumbers summations in (22) and (25) to be replaced by a trivial integral. Using expression (A11) it can be readily verified that the replacement

$$I_{\ell m}^k \approx \frac{1}{\sqrt{2}} \delta(q) \quad (A12)$$

is valid.

Numerical computation of the overlap integrals using the exact Bessel function solutions [Garrett and Munk, 1972] show that the accuracy of (A7) decreases with increasing frequencies reaching 40% at  $\omega/N_0 \sim .25$  (providing the modenumbers are greater than one). For  $q = 0$  the  $\mu_{\ell m}^k$

are typically less than 20% of the  $B_{\nu_{klm}}^2$ ; however, as  $q$  increases  $\nu$  decreases rapidly (see A11) while  $\mu$  is relatively constant.

# APPENDIX B

## ALTERNATIVE EXPRESSIONS FOR RELAXATION RATES

Equations (21) and (23) can be re-written in a form which makes transparent their relationship both to one another and to the familiar radiative transport equation of *Olbers* [1976], *McComas and Bretherton* [1977], and *Davidson* [1972].

To do this we use the hamiltonian coupling coefficients  $\Gamma_1(k; \ell, m)$  defined in I [Appendix A] and also the wave action variables (6). In terms of these the relaxation rates are

$$\begin{aligned} \langle J_{k\alpha} \rangle \hat{v}_F(k, \alpha) = 4\pi \sum_{\beta, \gamma} \sum_{\ell, m} \left\{ \frac{1}{2} |\Gamma_1(k; \ell, m)|^2 \delta_{\underline{k}-\underline{\ell}-\underline{m}} \delta(\omega_\alpha - \omega_\beta - \omega_\gamma) \right. \\ \left. + |\Gamma_1(m; k, \ell)|^2 \delta_{\underline{k}+\underline{\ell}-\underline{m}} \delta(\omega_\alpha + \omega_\beta - \omega_\gamma) \right\} \langle J_{\ell\beta} \rangle \langle J_{m\gamma} \rangle \quad (B1) \end{aligned}$$

$$\begin{aligned} \langle J_{k\alpha} \rangle v_P(k, \alpha) = 4\pi \sum_{\beta, \gamma} \sum_{\ell, m} \left\{ \frac{1}{2} |\Gamma_1(k; \ell, m)|^2 \delta_{\underline{k}-\underline{\ell}-\underline{m}} \delta(\omega_\alpha - \omega_\beta - \omega_\gamma) \right. \\ \times (\langle J_{\ell\beta} \rangle + \langle J_{m\gamma} \rangle) \langle J_{k\alpha} \rangle + |\Gamma_1(m; \ell, k)|^2 \delta_{\underline{k}+\underline{\ell}-\underline{m}} \delta(\omega_\alpha + \omega_\beta - \omega_\gamma) \\ \left. \times (\langle J_{\ell\beta} \rangle - \langle J_{m\gamma} \rangle) \langle J_{k\alpha} \rangle \right\} \quad (B2) \end{aligned}$$

Substitution of these expressions into  $v_B$  (24b) yields the usual expression.



The transport equation (29) can also be written in terms of action variables

$$\frac{d}{dt} \langle J_{k\alpha} \rangle = 2v_F(k, \alpha) [J_{k\alpha}^e - \langle J_{k\alpha} \rangle] \quad (B3)$$

where  $J^e$  is the equilibrium action. Equation (B3) can be generalized [Olbers, 1976] to include the effects of a mesoscale current  $U(x)$  by writing  $J_{k\alpha}(x)$ , and interpreting  $\frac{d}{dt}$  as

$$\begin{aligned} \frac{d}{dt} &= \frac{\partial}{\partial t} + \dot{x} \cdot \frac{\partial}{\partial x} + \dot{k} \cdot \frac{\partial}{\partial k} \quad , \\ \dot{x} &= \frac{\partial \Omega}{\partial k} \quad , \quad \dot{k} = - \frac{\partial \Omega}{\partial x} \quad , \quad \Omega = \omega_\alpha(k) + k \cdot U(x) \quad . \end{aligned} \quad (B4)$$

Table 1

Energy flow rates ( $\text{Wm}^{-2}$ ) from low modenumbers.

$\alpha$	$-\frac{dE_{\alpha}^{(-)}}{dt} \times 10^4$
1	1.1
2	1.3
3	1.3
4	1.1
5	1.0
6	0.6

$$\frac{dE^{(-)}}{dt} = \sum_{\alpha} \frac{dE_{\alpha}^{(-)}}{dt} = -6.4 (10)^{-4} \text{ Wm}^{-2}$$

# FIGURE CAPTIONS

- Figure 1* Resonance curves for dispersion relation (7). Dashed curves are for  $f = 0$ .
- Figure 2* Decay rate versus test wave frequency. Curves are labelled by modenumber. Dashed curve represents  $\nu_P = \omega_\alpha$ . GM-76 is used.
- Figure 3* Decay rate versus wavenumber for GM-76.
- Figure 4* Contours of  $\nu_P/N_0$  for GM-76. The shaded region indicates negative  $\nu_P$  corresponding to test wave growth.
- Figure 5* Comparison of  $\nu_B$  with  $\hat{\nu}_F$ . The quantity  $R$  [equation (30)] is plotted against test wave frequency for selected modenumber. GM-76.
- Figure 6* Comparative equilibria for different wavenumber slopes  $p$  of PSD (10). GM-76 uses  $p = 2$ . Non-equilibrium regions ( $R > 0.1$ ) are shaded and the sign of  $\nu_B$  is given. Otherwise contours of  $R$  are drawn: Dashed contours denote  $R = 10^{-2}$ , dots denote  $R = 10^{-3}$ .
- Figure 7* Comparative equilibria for different modenumber slopes  $t$  of PSD (10). GM-76 uses  $t = 2$ .

*Figure 8* Comparison between the dominant induced diffusion transfer mechanism [equation (36)] and the full numerical calculation of  $v_p/N_o$ . Curves are labelled by modenumber.

*Figure 9* Comparison of contributions to  $|v_p|/N_o$  from special transfer mechanisms. Analytic expressions for induced diffusion [equation (36) ——— ], elastic scattering [equation (37) - - - - - ] and modified parametric subharmonic instability [equation (41) — • — • — • ] are evaluated. Curves are labelled by modenumbers.

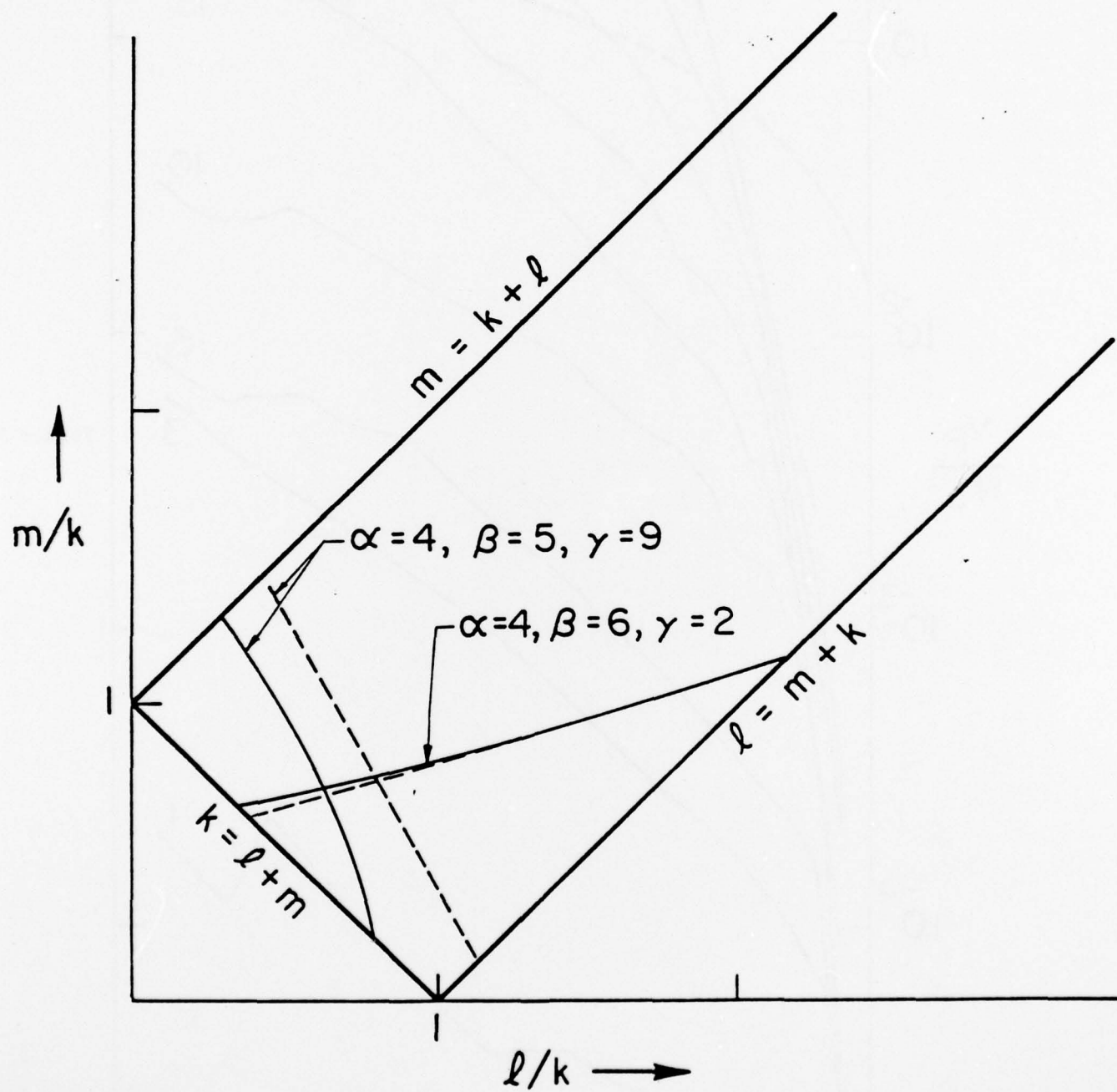


Figure 1



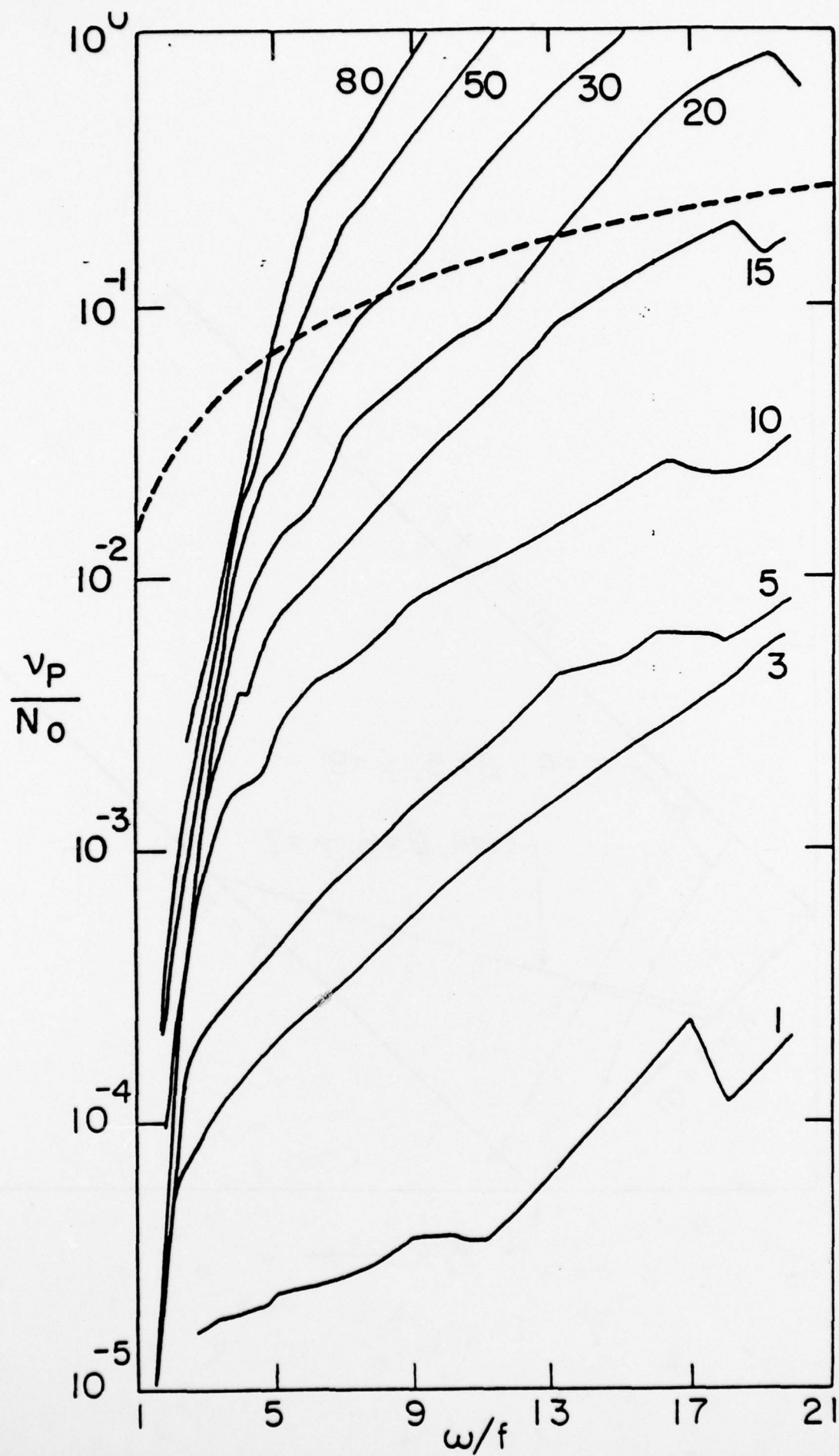


Figure 2

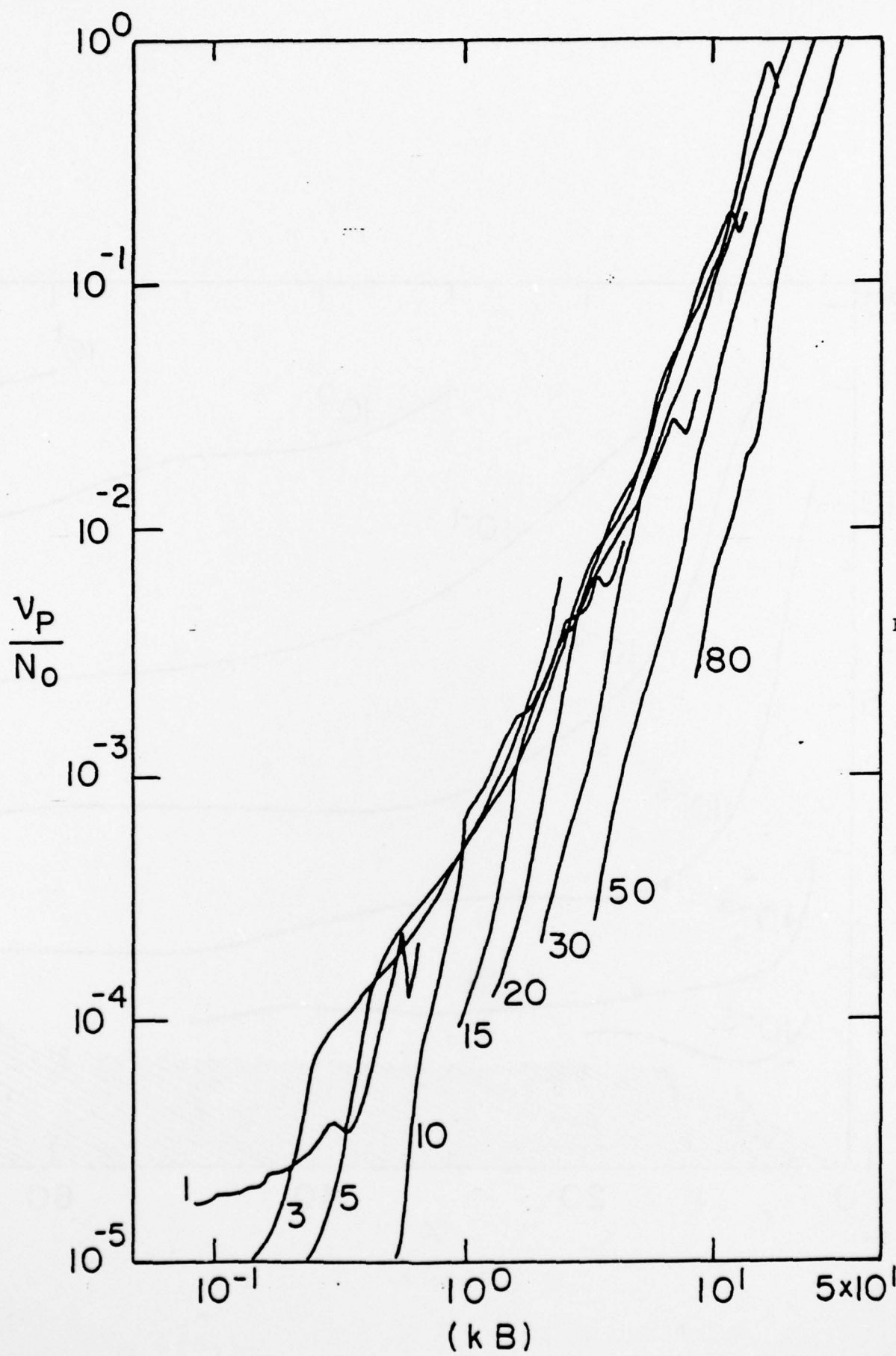


Fig. 3

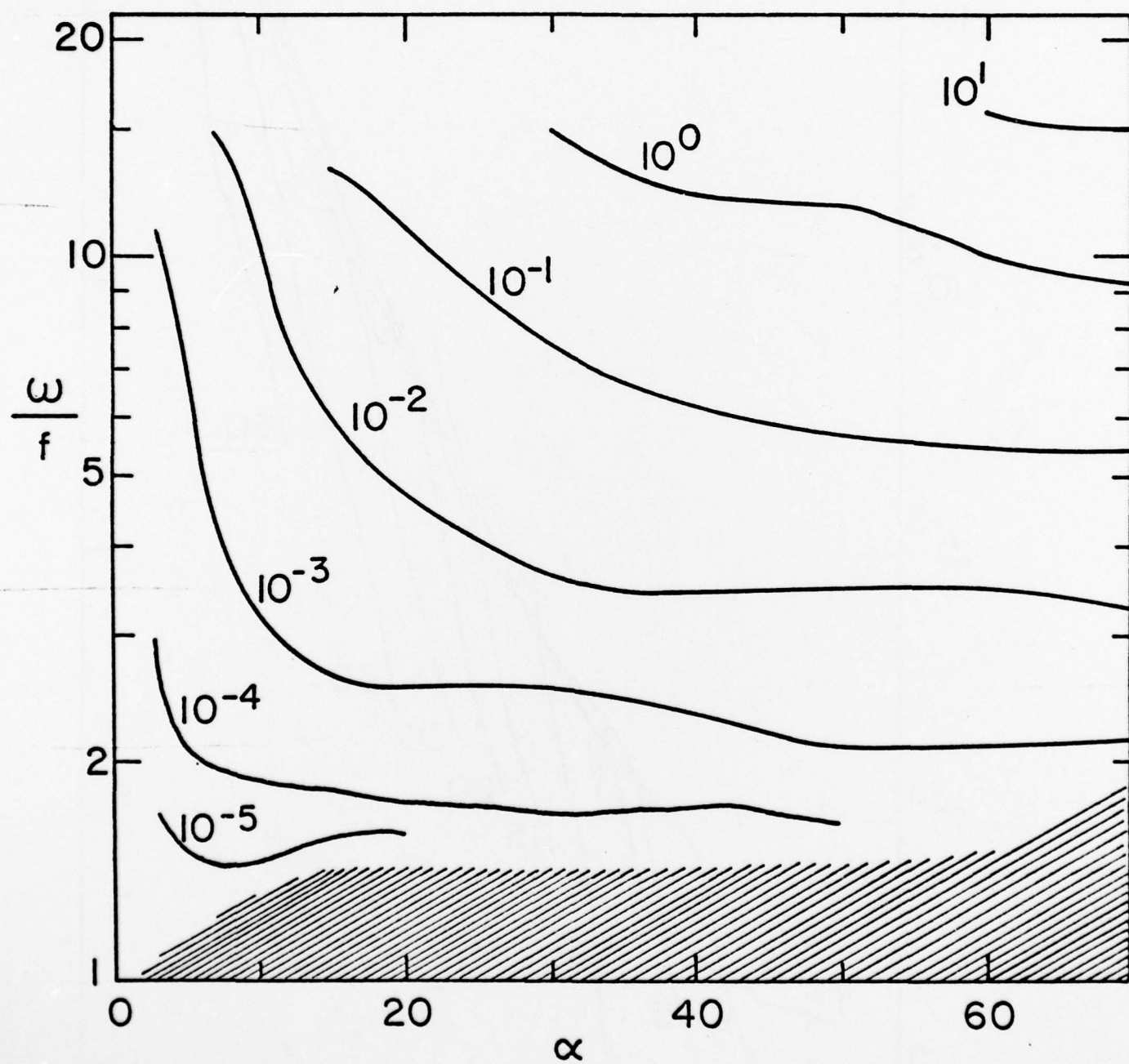


Figure 4

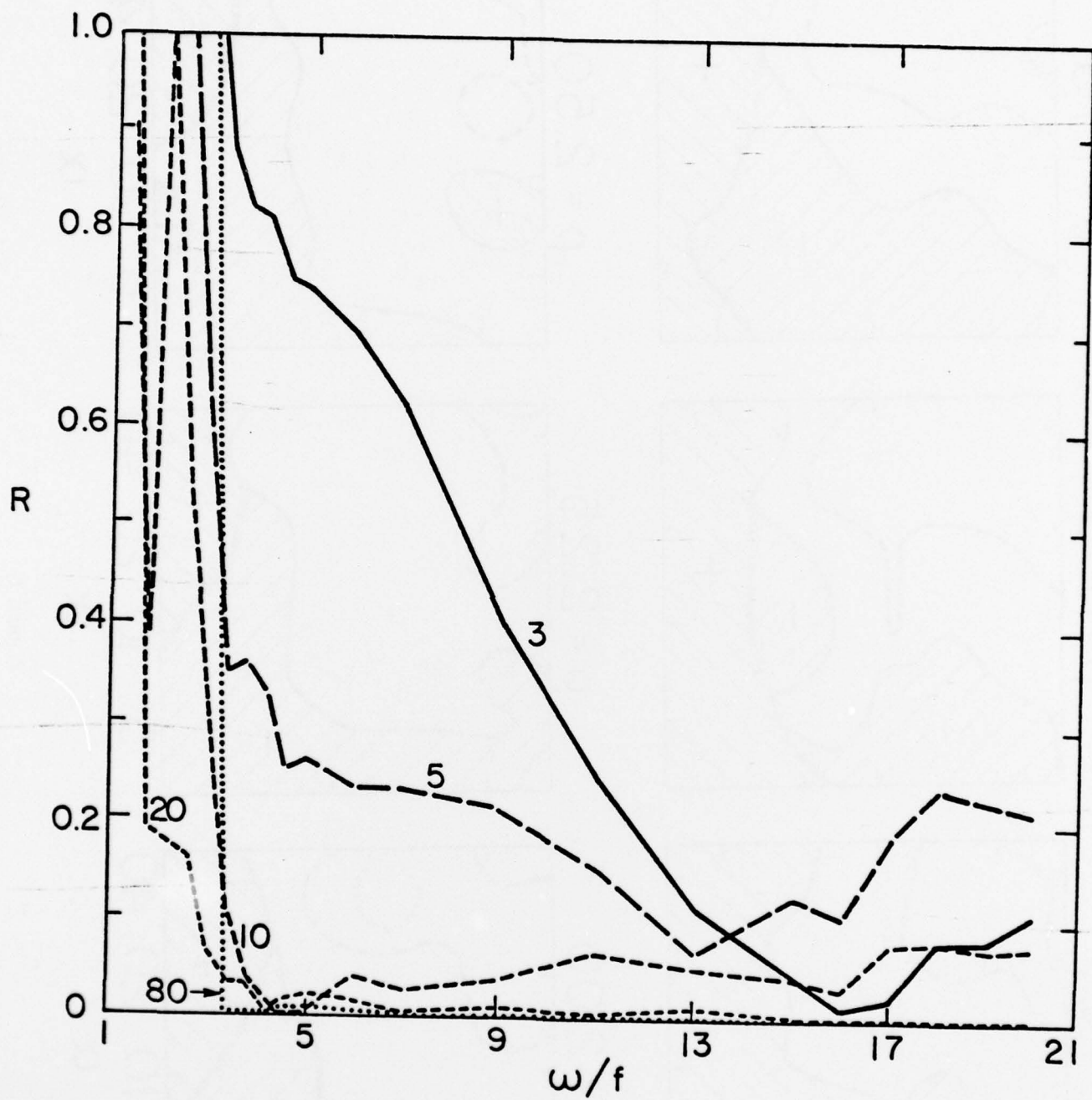


Figure 5



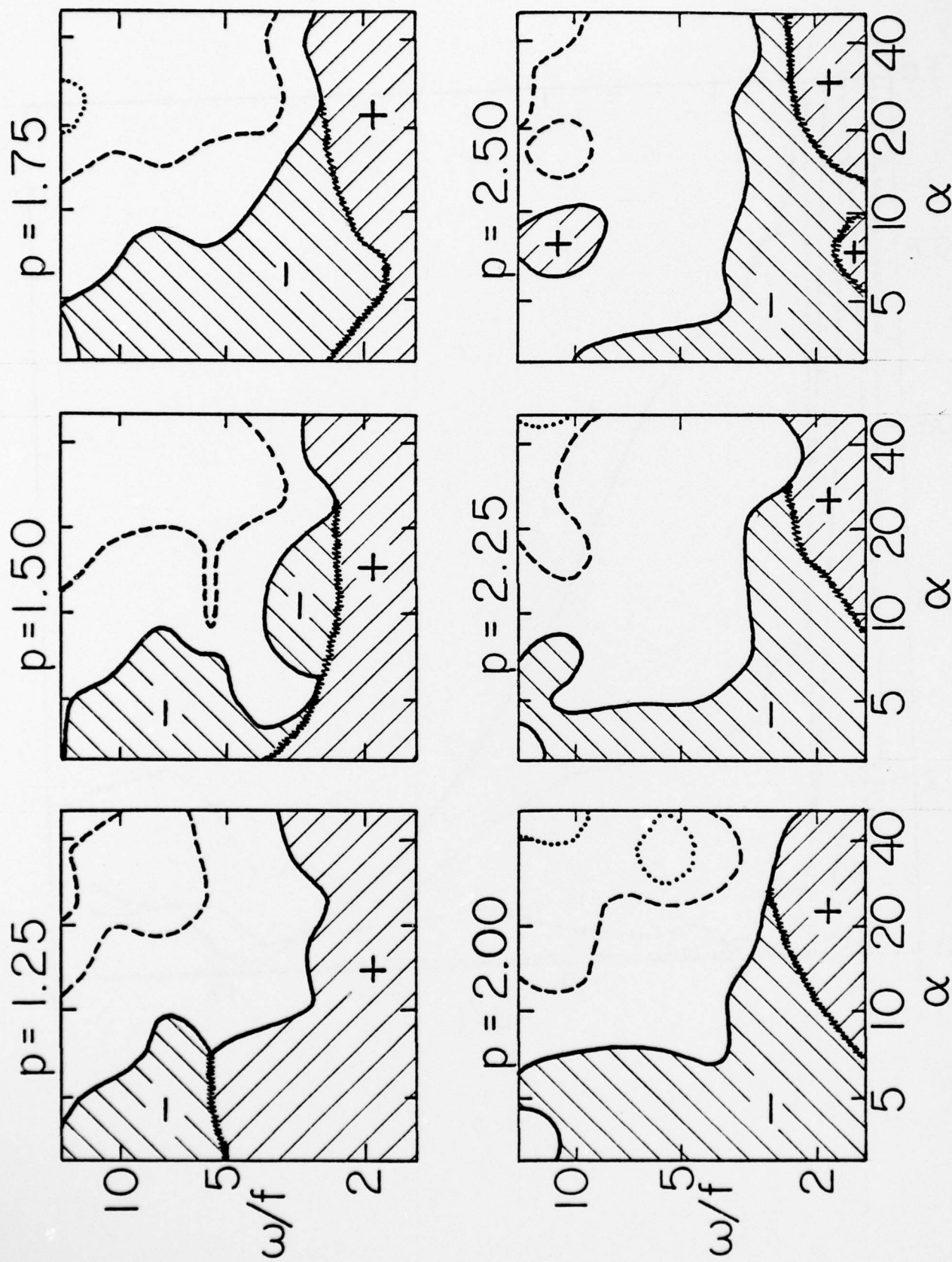


Figure 6



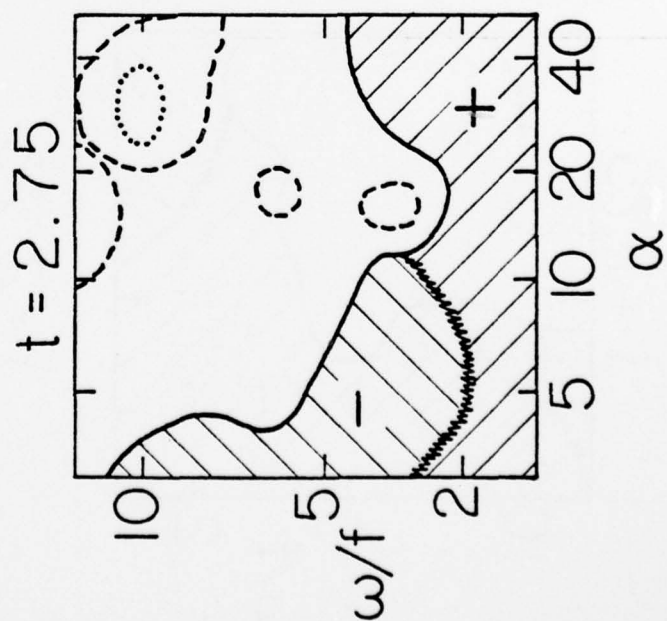
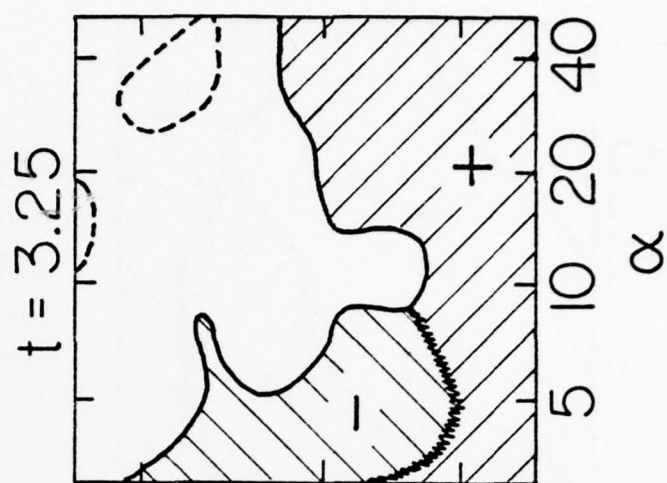
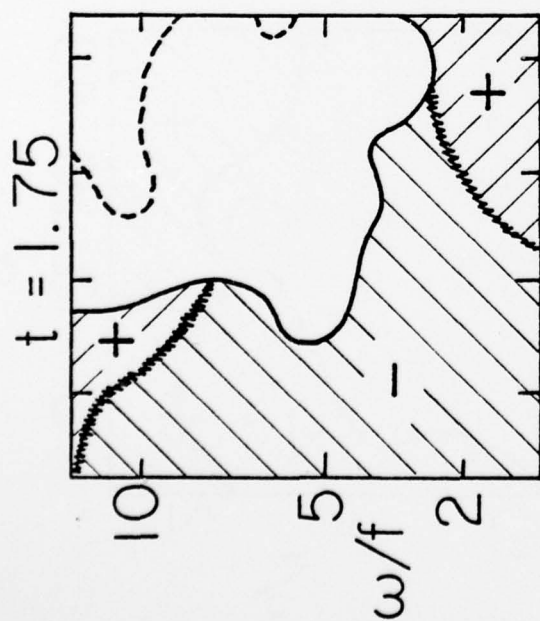
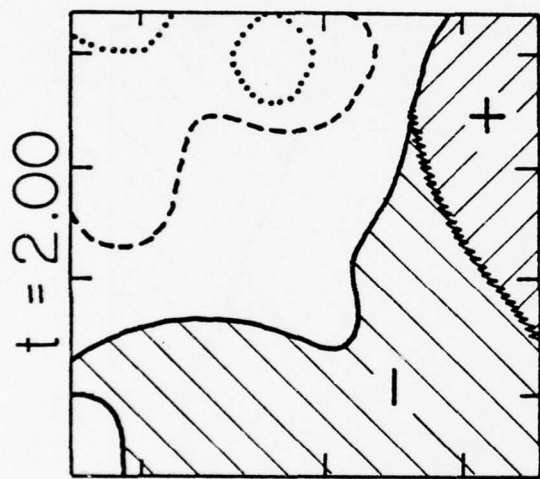
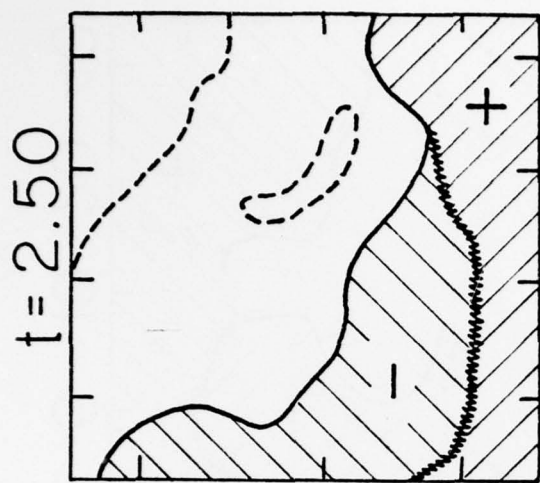


Figure 7

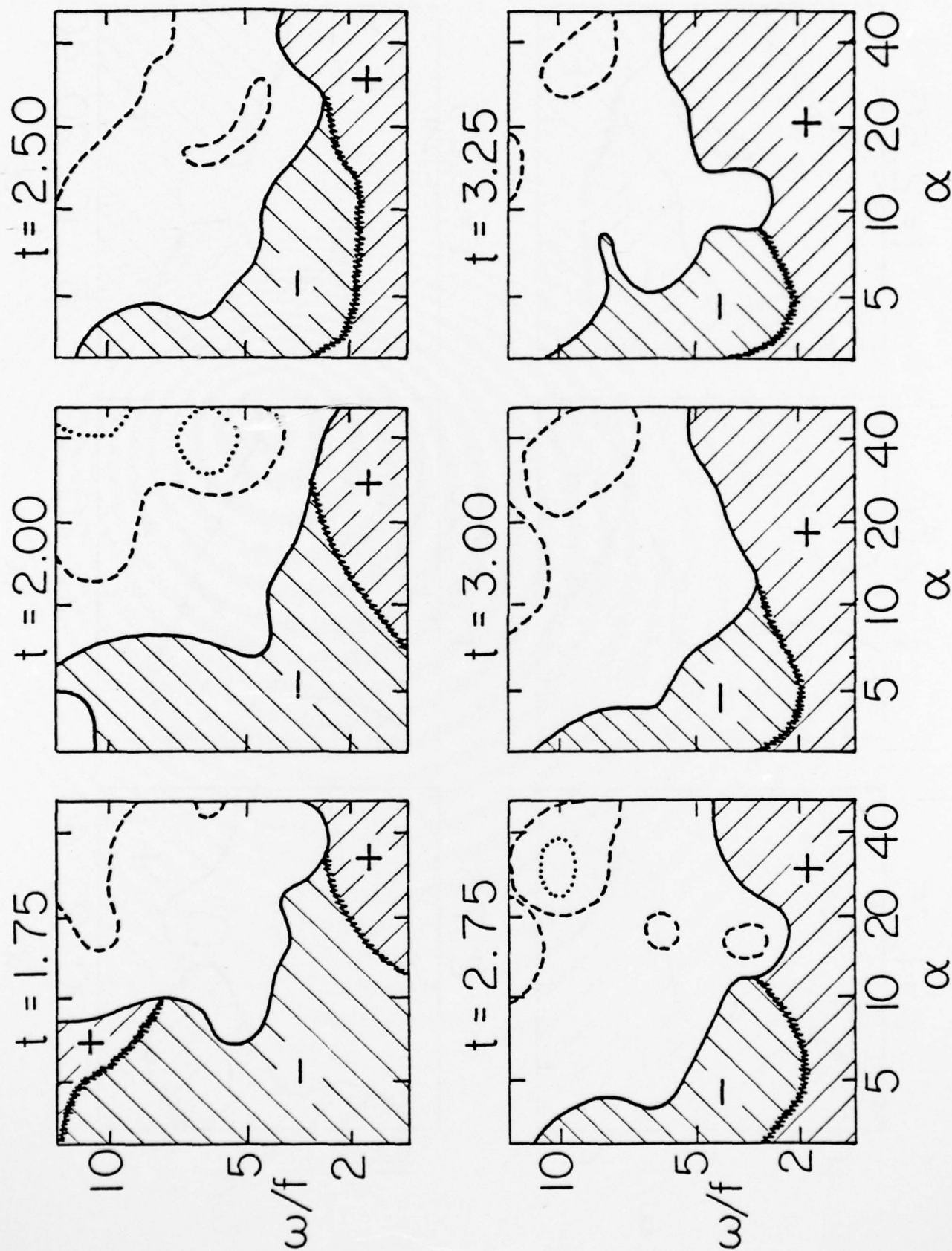


Figure 7

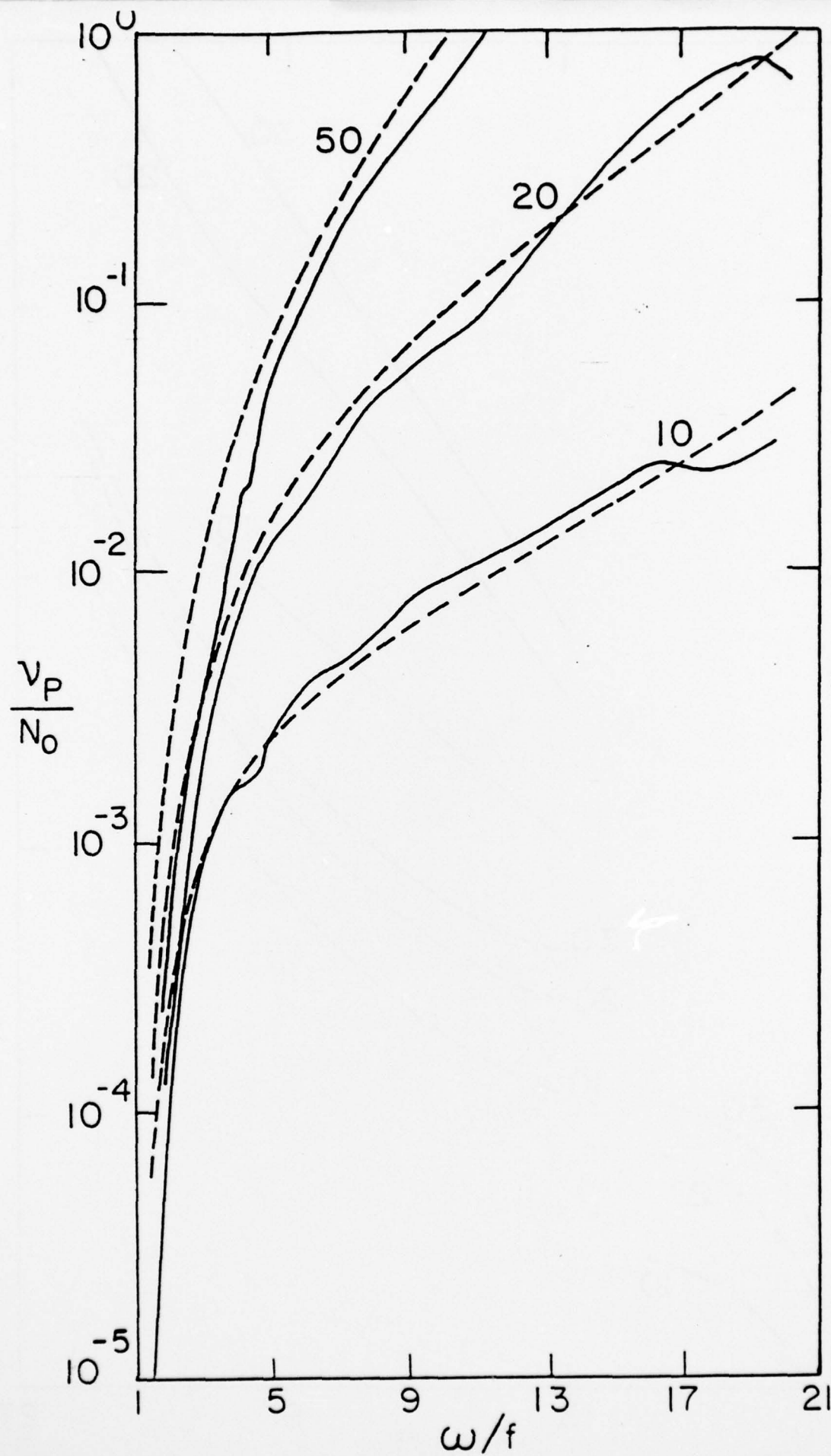


Figure 8

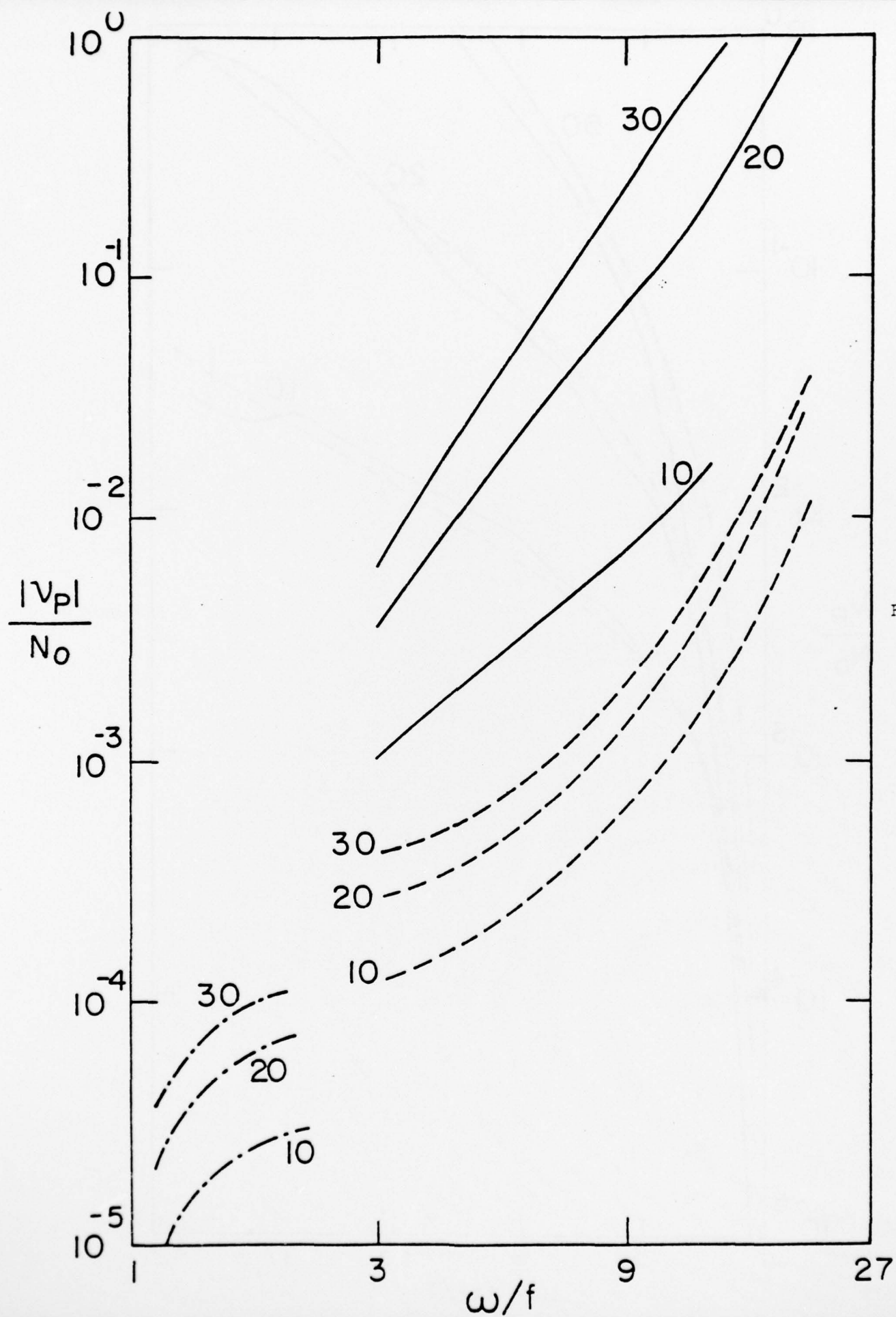


Figure 9